Electronic Supplementary Material (ESI) for Physical Chemistry Chemical Physics.

Thermostable water reservoirs in the interlayer space of a sodium hectorite clay through the intercalation of γ-amino-propyl(dimethyl)ethoxysilane in toluene.

Waldemar Keil, Kai Zhao, Arthur Oswald, Wolfgang Bremser, Claudia Schmidt and Horst Hintze-Bruening*

Paderborn University, Department of Chemistry, Warburger Str. 100, D-33098 Paderborn, Germany

Supporting Information

TGA

TGA traces for the LAP and MMT series are shown in Figure S1. Note that the second step around 200 °C for AP*M*S@LAP is identified as H_2O by means of TGA-MS (figure S2).

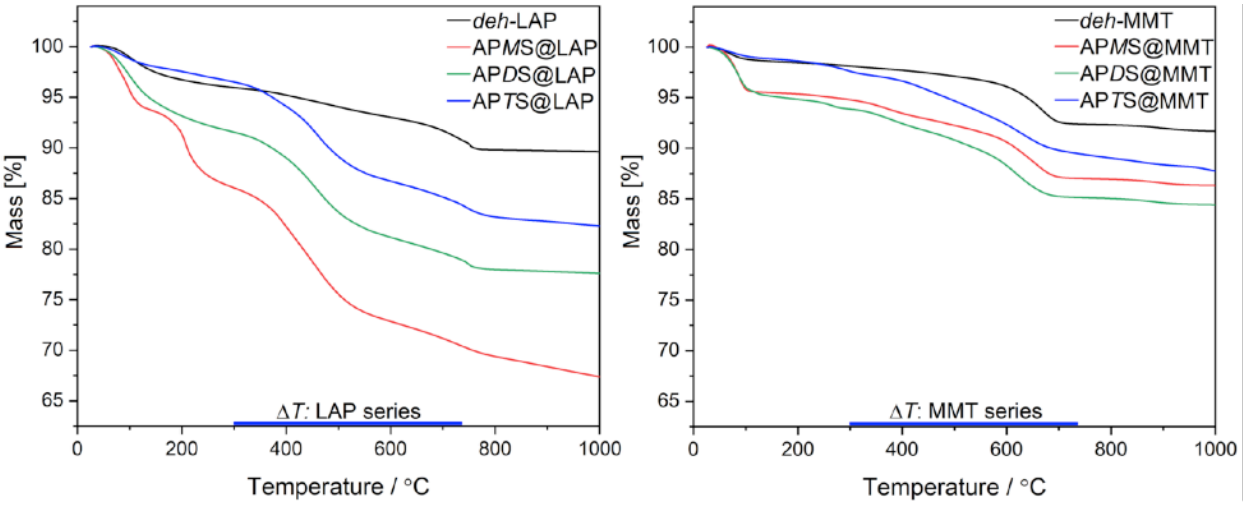

Figure S1: TGA traces for the LAP and MMT series. Blue bars at the bottom indicate the temperature ranges used for the calculation of the silylation yields. The curves of AP*T*S@LAP, AP*T*S@MMT and AP*M*S@LAP don't reach a plateau at 1,000 °C for technical reasons (cf. experimental section of the manuscript).

TGA-MS

By means of mass spectrometry, combustion products from TGA and dTGA can be quantified and assigned to their m/z ratio. In Figure S2 and S3, temperature dependent ion current intensities are shown for a variety of ions, for the LAP and MMT series. Note, that the ion current intensities for different m/z traces cover up to five orders of magnitude and individual traces of the combustion products should be taken semi-quantitatively.

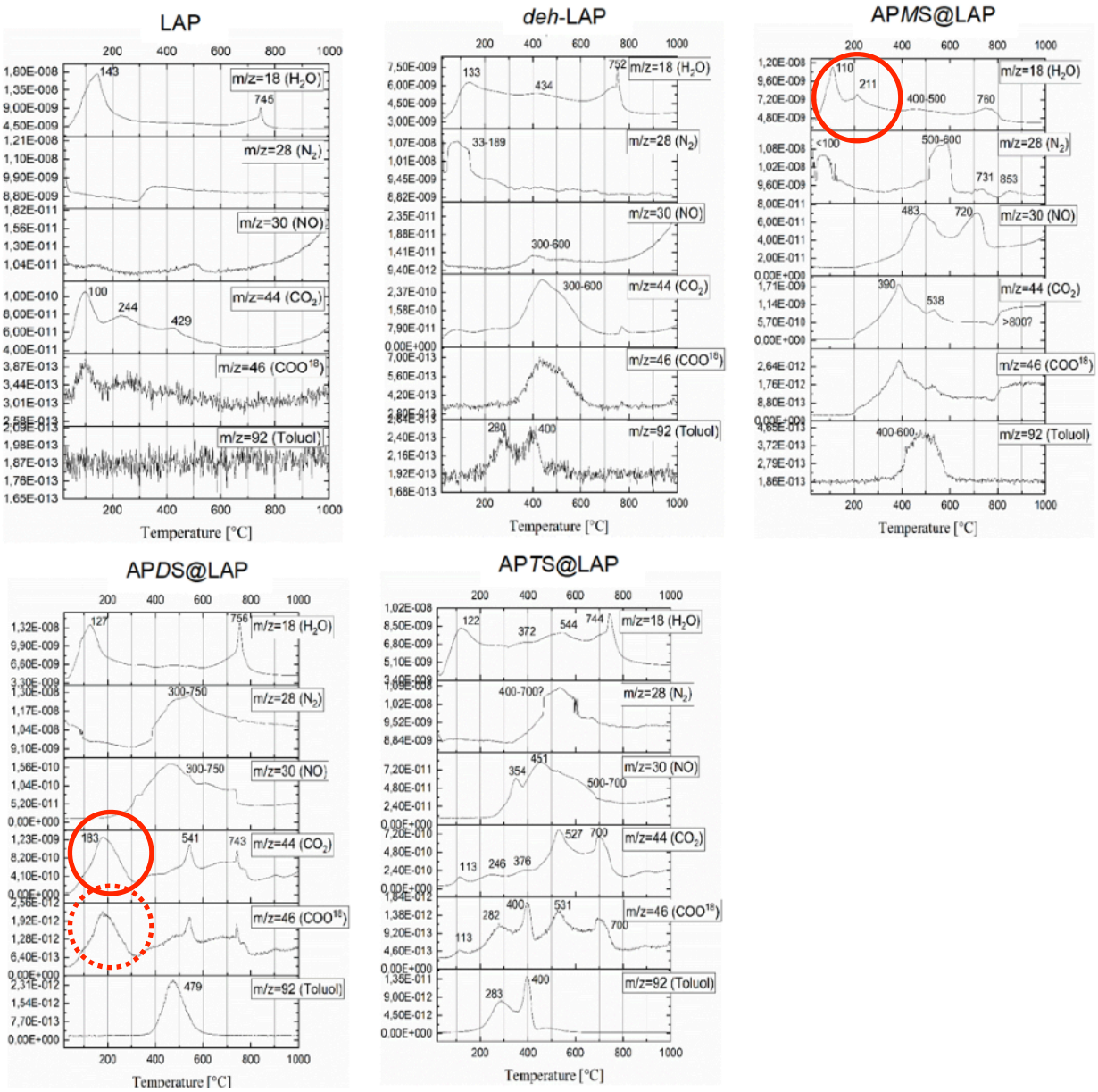

Figure S2: Temperature dependent ion-current intensities for the LAP series. Note the second peak at 211 °C for m/z = 18 in AP*M*S@LAP for released H_2O and the peaks at 183 °C for m/z = 44 & 46 in AP*D*S@LAP for released CO_2 and $C^{18}OO$, respectively. Note: the molecular mass of ethanol is 46.

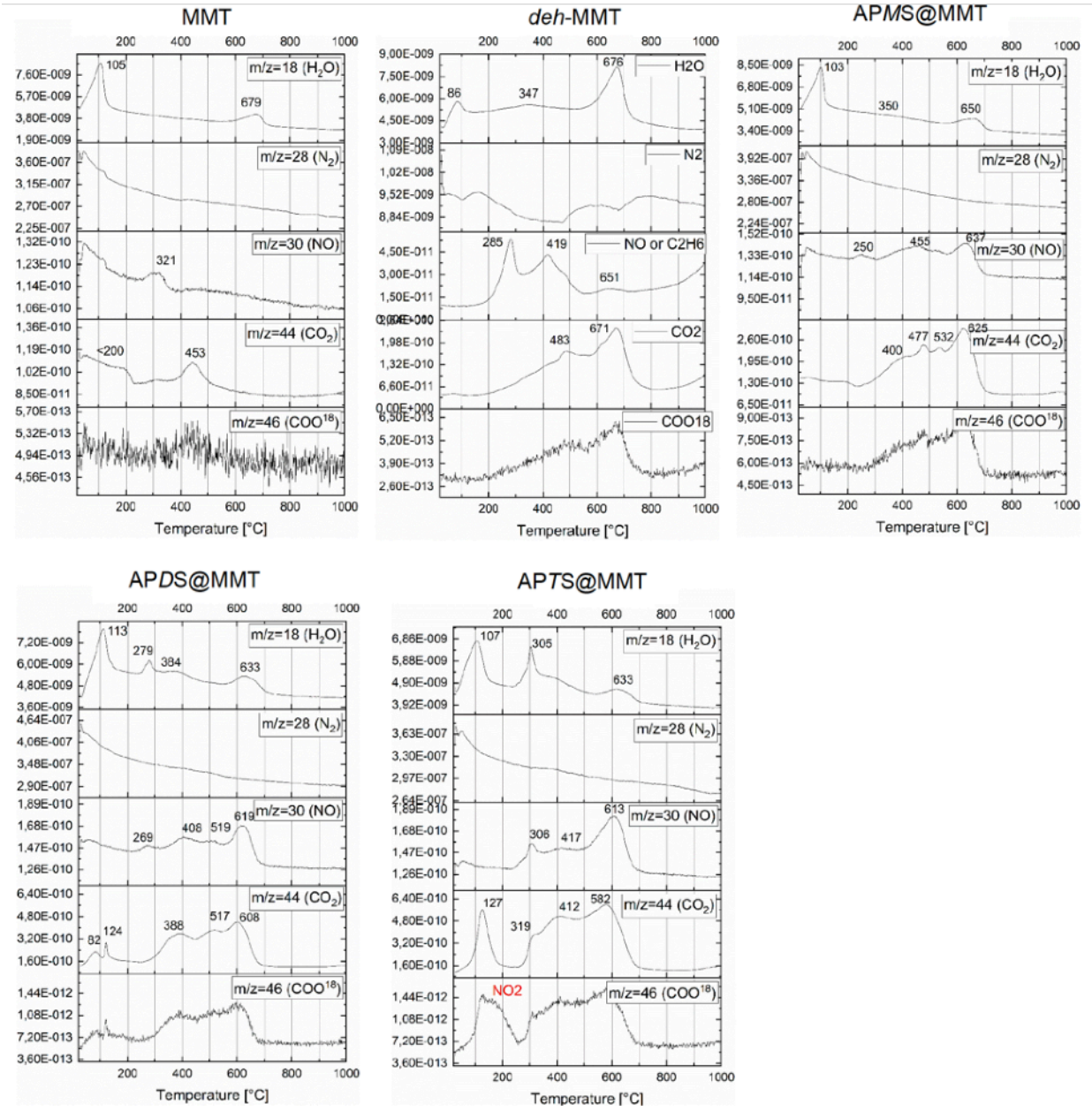

Figure S3: Temperature dependent ion-current intensities for the MMT series.

XRD

The small angle sections of XRD curves for the sample AP*M*S@LAP (annealed at 200 °C) and AP*M*S@LAP tel quel are compared in Figure S4. The maximum of the 001 reflection is shifted to larger 2θ values after annealing the sample at 200 °C.

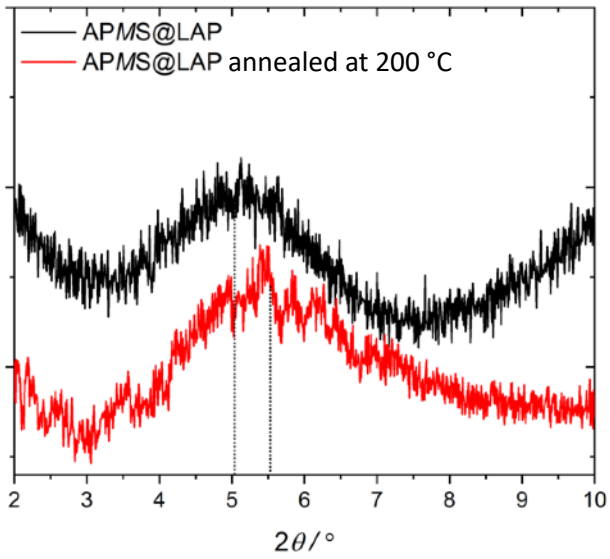

Figure S4: XRD small angle section of AP*M*S@LAP and AP*M*S@LAP (annealed at 200 °C).

EDX

The outcome of the elemental analysis by EDX is summarized in Table S1. Notably, an iron content of approximately 2 atom-% can be found for MMT-based samples.

Table S1: Element content of bare and modified LAP and MMT based on EDX.

Samples	Si/Mg	N/%	Fe/%
Laponite	1.64	0.00	0.11
AP*M*S@LAP	1.98	0.61	0.04
AP*D*S@LAP	2.05	1.36	0.02
AP*T*S@LAP	1.74	1.08	0.06
MMT	2.48	0.17	1.96
AP*M*S@MMT	2.57	0.20	1.33
AP*D*S@MMT	2.71	0.69	1.52
AP*T*S@MMT	2.85	1.20	1.26

^{29}Si NMR Herzfeld-Berger Analysis

A Herzfeld-Berger analysis of the spinning side bands has been carried out for the ^{29}Si signals of the Q^3 groups of neat LAP and MMT in order to estimate the principal values of the chemical shift tensors (cf. figure 5 of the main text). Due to overlapping signals from different sites this analysis is approximative and serves only to estimate how much LAP and MMT differ in the chemical shift anisotropy of the Q^3 groups. For bare LAP the principal values are −97.2, −92.6 and −92.6, whereas for bare MMT they are 7.2, −94.7 and −196.6.

^{23}Na NMR

Two sets of ^{23}Na NMR spectra for different samples of LAP and MMT are shown in Figure S5. The clay samples were measured as received, oven dried for 12h at 120 °C ("od") and after stirring in toluene and subsequent drying for 12h at 120 °C ("*deh*"). This shows that the solvent has an impact on the sodium cations in LAP which is basically absent in MMT.

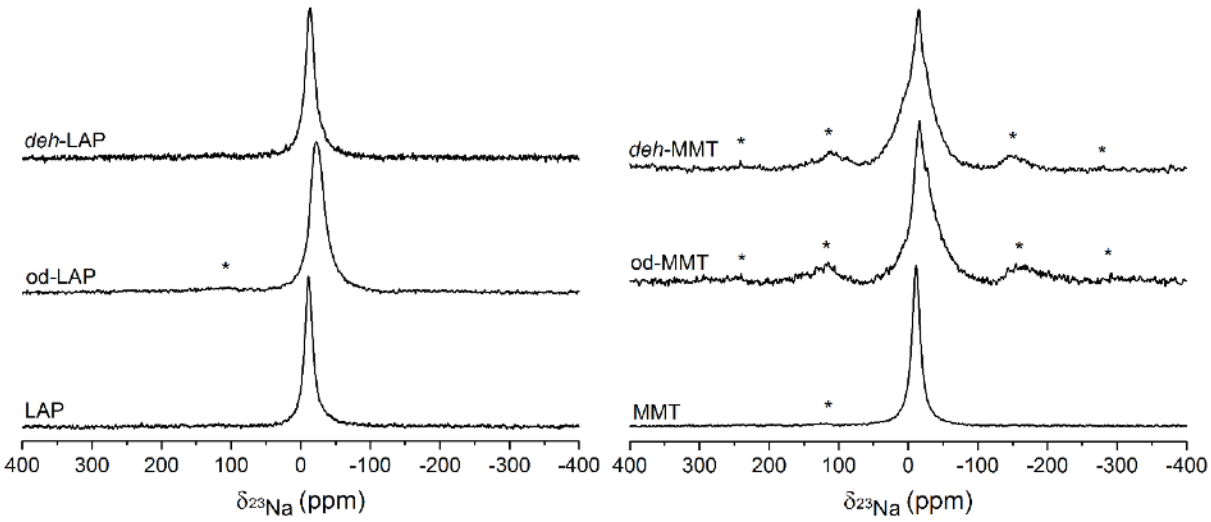

Figure S5: ^{23}Na NMR spectra of different LAP and MMT samples. Spectra were obtained under MAS at 10 kHz.

^{7}Li NMR

Figure S6 shows the ^{7}Li MAS spectra of the LAP series, featuring the central transition and the spinning sidebands (spanning a range of c. 30 kHz) of the satellite transitions. No significant differences can be found throughout the sample series.

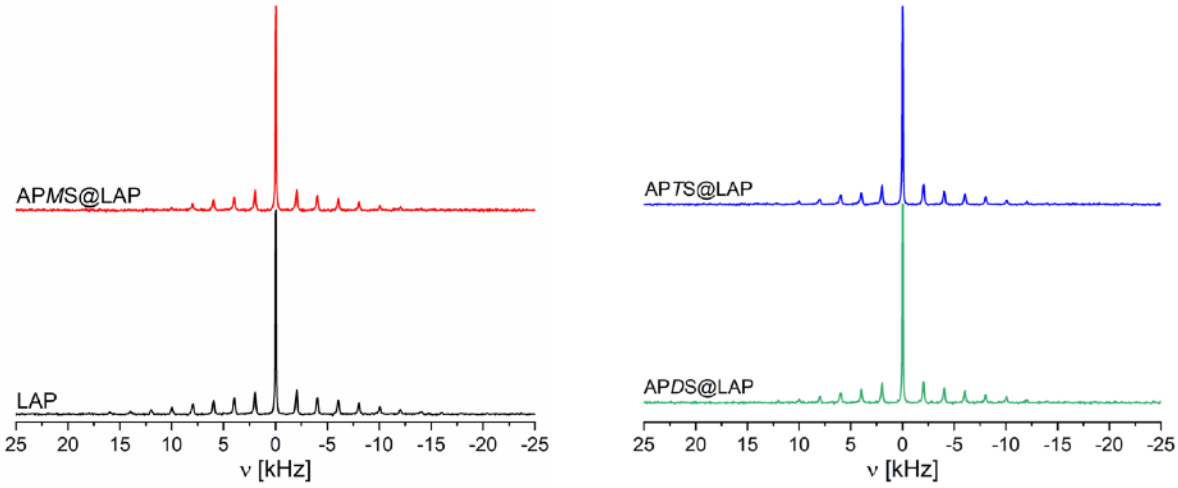

Figure S6: ^{7}Li NMR spectra of the LAP series, obtained under MAS at 2 kHz. LAP is bare LAP.

^{27}Al NMR

Figure S7 shows the ^{27}Al MAS spectra of the MMT series. Minor differences in signal intensities can be noted for the fourfold coordinated Al sites. This proves isomorphous substitution of Si by Al which contributes to the negative layer charge in MMT (besides isomorphous substitution of Al by Mg in the octahedral sites).

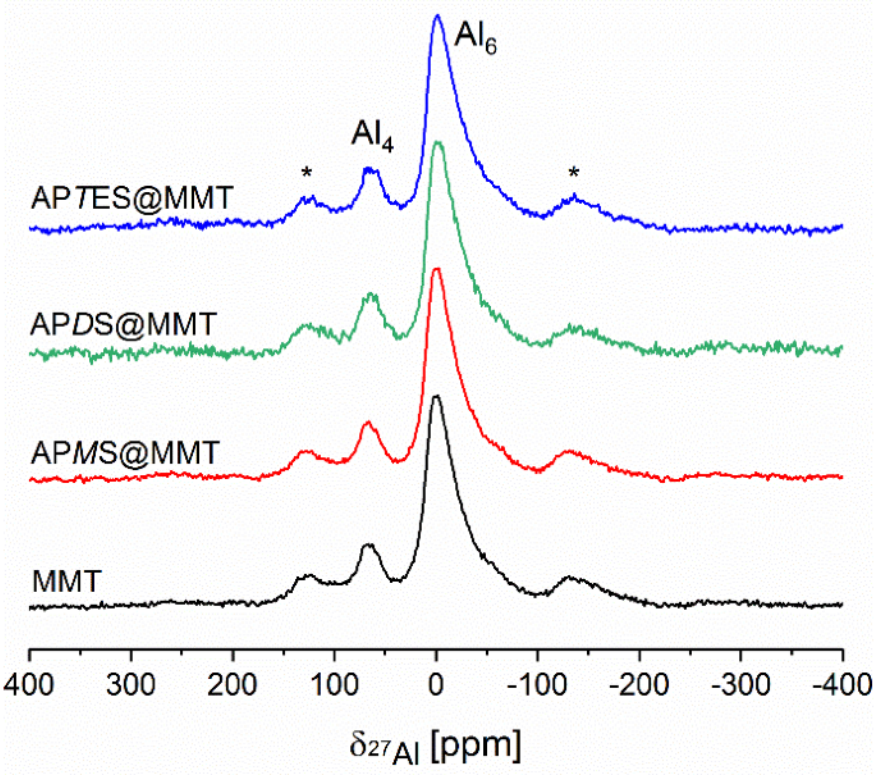

Figure S7: ^{27}Al NMR spectra of the MMT series, obtained under MAS at 10 kHz and proton decoupling. Al_4 and Al_6 denotes four- and sixfold coordinated Al.

Zeta-Potential

The respective conductivities and count rates from the zeta-potential measurements shown in table 1 of the main text are listed in Table S2.

Table S2: Conductivity and count rate of bare and modified LAP and MMT.

Samples	**conductivity (mS/cm)**	**count rate (Kcps)**
bare Laponite	0.179	51.4
AP*M*S@LAP	0.114	360.1
AP*D*S@LAP	0.091	276.1
AP*T*S@LAP	0.125	95.8
bare MMT	0.123	230.1
AP*M*S@MMT	0.131	194.7
AP*D*S@MMT	0.094	259.7
AP*T*S@MMT	0.142	476.2

BET Surfaces

The nitrogen physisorption measurements were conducted on an Autosorb 6B from Quantachrome at 77 K. Prior to the measurement the samples were degassed at 120 °C in vacuum for 12 h. The BET surface area was determined by linear regression in the relative pressure range between 0.1 and 0.3. The BET results are summarized in Table S3. The significant difference in specific surface between Laponite® and MMT can be explained by the difference in aspect ratio. Upon modifying Laponite® and MMT with one of the three amino-silanes, a reduction in specific surface can be noted, indicating that the interlayers are blocked by the amino-silanes. For AP*T*S@MMT, we tested some post-treatments, which lead to a reincrease of the specific surface area.

Table S3: Specific surface areas (BET) of bare and modified LAP and MMT.

Samples	S_{spec} **(m²/g)**	**Samples**	S_{spec} **(m²/g)**
bare Laponite	379	**bare MMT**	49
AP*M*S@LAP	12	AP*M*S@MMT	14
AP*D*S@LAP	3	AP*D*S@MMT	14
AP*T*S@LAP	48	AP*T*S@MMT	3
		AP*T*S@MMT (ht-oven)	9
		AP*T*S@MMT (fd)	16
		AP*T*S@MMT (ht-fd)	24

ht: hydrothermal treatment in a PTFE-lined stainless-steel bomb
fd: freeze-drying
oven: drying at 120°C for 12h

SEM Images

In Figure S8 SEM images of the clay morphology on a silicon wafer after drying an aqueous 1 wt.-% clay dispersion are shown.

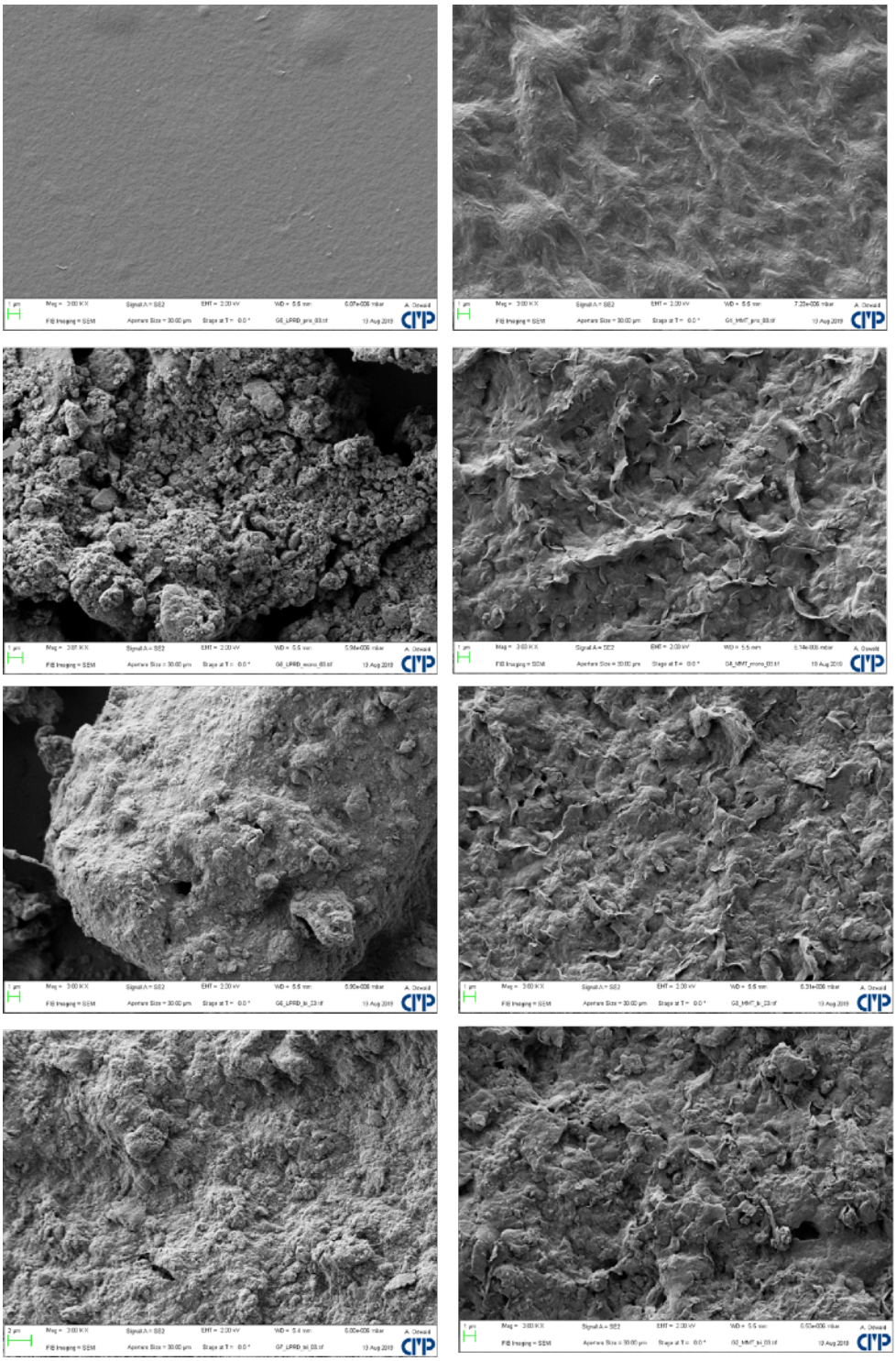

Figure S8: Morphologies of clays imaged via SEM; *left column*, *from top to bottom*: bare LAP, AP*M*S@LAP, AP*D*S@LAP, AP*T*S@LAP; *right column: the* respective clay and hybrids of the MMT series.